Analog Signal Transmission in a High-Contrast-Gratings-Based Hollow-Core-Waveguide

H. Huang, Y. Yue, L. Zhang, C. Chase, D. Parekh, F. Sedgwick, M. C. Wu, C. J. Chang-Hasnain, M. Tur, and A. E. Willner

***Abstract*—In this paper, the performance of an on-chip hollow-core-waveguide (HW) using high-contrast gratings (HCG) for analog signal transmission is analyzed numerically. Simulation results indicate that after propagating 100 m in a HCG-HW with optimally designed parameters, there is very little degradation of either third-order intermodulation distortion spur-free dynamic range (IM3 SFDR) or third-order harmonic distortion (THD) SFDR. Due to the chromatic dispersion of the HCG-HW, the highest second-order harmonic distortion (SHD) SFDR is limited to 107.3 dB $\cdot$Hz$^{1/2}$. In addition, $>$100 dB $\cdot$Hz $^{2/3}$ IM3 SFDR can be achieved over a radio frequency (RF) range of 80 GHz and an optical wavelength bandwidth of 50 nm after propagation 100 m through a HCG-HW. The parameter dependence of the waveguide performance is also investigated. With a $\pm$20 nm variation on all parameters, the propagation length in an HCG-HW is limited to $\sim$6 m in order to maintain an IM3 SFDR of $>$100 dB $\cdot$Hz $^{2/3}$.**

***Index Terms*—Dynamic range, harmonic distortion, intermodulation distortion, microwave photonics, integrated optical waveguides.**

I. Introduction

WAVEGUIDE structures are used for many elements and components inside photonic integrated circuits (PICs). For on-chip photonic links, it is important to maintain the linearity of the transmitted signals, especially for analog signals [1], [2]. However, it is extremely difficult to achieve this goal by using regular integrated waveguides due to their large loss, dispersion and nonlinearity. Hollow-core-waveguides (HWs) have been shown to exhibit extremely low nonlinearity as well as low loss and high thermal stability, all of which are important characteristics for analog elements [3]. Moreover, high-contrast gratings (HCGs) can provide extremely large reflectivity over a broad bandwidth, and they have been used to confine the light wave in the hollow core. It seems that the hollow core waveguide using HCG may have the potential to further reduce the propagation loss [4].

Manuscript received February 22, 2012; revised July 25, 2012; accepted September 30, 2012. Date of publication October 19, 2012; date of current version December 08, 2012. This work was supported in part by the Defense Advanced Research Projects Agency (DARPA) Integrated Photonic Delay (iPhoD) program (under contract numbers HR0011-09-C-0124).

H. Huang, Y. Yue, L. Zhang and A. E. Willner are with the Department of Electrical Engineering, University of Southern California, Los Angeles, CA, 90089, USA. (E-mail: haoh@usc.edu).

M. Tur is with the School of Electrical Engineering, Tel-Aviv University, Tel-Aviv, 69978, ISRAEL.

C. Chase, D. Parekh, F. Sedgwick M. C. Wu and C. J. Chang-Hasnain are with the Department of Electrical Engineering and Computer Sciences, Univ. of California, Berkeley, CA, 94720, USA.

Color versions of one or more of the figures in this paper are available online at http://ieeexplore.ieee.org.

Digital Object Identifier 10.1109/JLT.2012.2224844

For an HCG with optimized design, the light propagation in the hollow region excites modes in the grating bars. The first two excited modes can cancel one another outside the gratings, which leads to extremely high reflectivity [5]. Recently, it is indicated that HCG waveguides may exhibit extremely low nonlinearity under a wide variety of waveguide parameters [6]. However, both loss and chromatic dispersion can vary significantly with the variation of waveguide parameters and might affect the operation of an analog link or subsystem [7]. Therefore, it might be desirable to characterize the HCG-HW for their suitability in microwave analog applications.

In this paper, we analyze the analog signal performance of hollow-core waveguides using HCGs [8]. The link SFDR of the third-order intermodulation distortion (IM3), second-order harmonic distortion (SHD) and the third-order harmonic distortion (THD) are calculated. After propagating 100 m in a HCG-HW with optimally designed parameters, there is very little degradation with respect to the back-to-back case of either third-order intermodulation distortion spur-free dynamic range (IM3 SFDR) or third-order harmonic distortion (THD) SFDR [9]. The simulation results also indicate that a HCG-HW analog link potentially can operate at modulation frequencies of up to 80 GHz, and in an optical bandwidth of $>$50 nm, while maintaining an IM3 SFDR of $>$100 dB$\cdot$ Hz $^{2/3}$. The impact of parameter variations of an HCG-HW on the linearity of the link also is investigated. With $\pm$10 nm and $\pm$20 nm variations on all parameters, the propagation length in an HCG-HW is limited to $\sim$28 m and $\sim$6 m, respectively, in order to maintain an IM3 SFDR of $>$100 dB $\cdot$ Hz$^{2/3}$.

II. Waveguide Parameters

The two-dimensional structure of an HCG-HW is shown in Fig. 1. High contrast silicon gratings with refractive indices of 3.476 are surrounded by air, which has a low refractive index, thereby providing a very high reflectivity ($>$99.9%) [10]. Two layers of HCG, placed parallel to each other, function as two mirrors and light can be confined effectively within the hollow core. Therefore, it is expected that low nonlinearity and loss can be achieved by this structure, since most of the energy of the light is confined and transmitted in the air (hollow-core). It is noted that four parameters have significant effects on the performances of an HCG-HW, i.e., core size (D), period (Λ), air gap (a_g) and thickness (t_g). Core size is the distance between the two layers of HCGs. The other three parameters are related to the grating structure, as shown in Fig. 1. An HCG-HW that has been optimized for low loss, i.e., thickness of 340 nm, period of 750 nm, air gap of 430 nm and core size of 15 μm, can achieve a propagation loss as low as 0.0052 dB/m [6]. Fig. 2(a) depicts

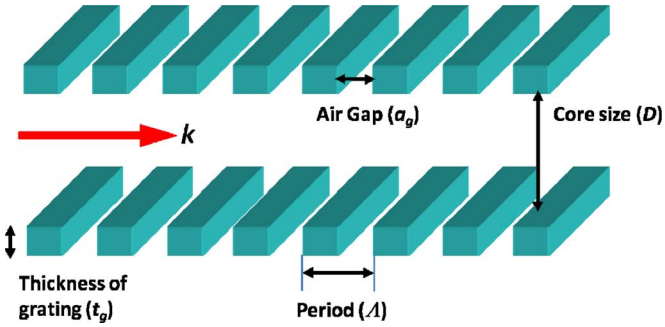

Fig. 1. Two-dimensional structure of an HCG-HW. $\boldsymbol{k}$ indicates the propagation direction of the confined lightwave.

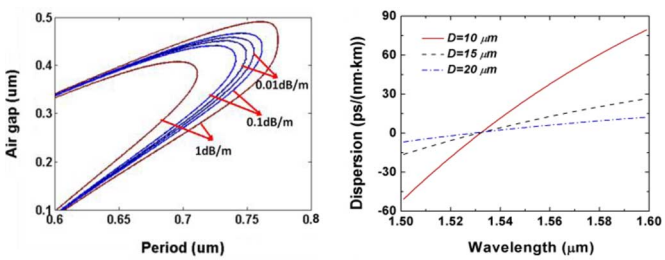

(a) (b)

Fig. 2. (a) Calculated waveguide loss (dB/m) at 1550 nm for an HCG-HW with a 15 μm core size as a function of grating period and air gap. (b) Chromatic dispersion of HCG-HW as a function of wavelength. D : core size of the HCG-HW.

the loss contour within the range of 1 dB/m for an HCG-HW with a core size of 15 μm. An HCG-HW with >50 nm variations in its grating thickness and its air gap can still provide a loss of <1 dB/m. Fig. 2(b) also shows that a chromatic dispersion of <100 ps/(nm $\cdot$ km) can be achieved over a wavelength range of 100 nm and the dispersion can be even lower if the core size is increased.

III. Link Modeling

A. HCG-HW Analog Optical Link

The schematic configuration of the analysis model is shown in Fig. 3. A continuous wave (CW) at 1550 nm is generated by a laser source with a linewidth of 1 kHz and a relative intensity noise (RIN) of -165 dB/Hz. The output power of the CW laser is 20 dBm. Then the CW is double-sideband-modulated by analog signals (two sine waves with frequencies very close to each other, e.g., 40 GHz and 41 GHz), using a quadrature-biased Mach-Zehnder modulator (MZM) with a V_π of 5 V. The modulated optical signal is then launched into the HCG-HW for signal transmission. After optical-to-electrical conversion by a PIN photodetector with a responsivity of 0.7 A/W, the output signal is analyzed in terms of harmonic and intermodulation distortions. The common parameters used in the modeling are organized into Table I.

B. SFDR

SFDR is an important common measure of the linearity of an analog link [1], [2]. It is defined as the RF input power range,

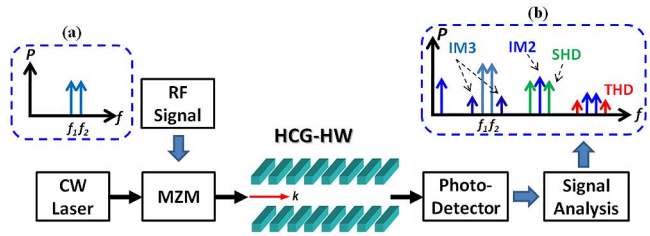

Fig. 3. Schematic of an analog link using HCG-HW. Insets (a) and (b) describe the spectra of the input RF signal and the output RF signal after transmission in HCG-HW, respectively.

TABLE I
HCG-HW Optical Link Common Parameters

CW Laser	Laser Power	20	dBm
	Laser Noise (RIN)	-165	dB/Hz
	Wavelength	1550	nm
Electro-optical Modulator	V_π	5	V
	Modulator Impedance	50	Ω
	Insertion Loss	3	dB
	Fundamental frequencies (f_1, f_2)	f_1=40, f_2=41	GHz
Waveguide structure	Core size	15	μm
	Period	750	nm
	Air gap	430	nm
	Thickness	340	nm
	Length	100	m
PIN Photo detector	Detector load	50	Ω
	Detector responsivity	0.7	A/W
	Dark current	1	nA
Noise bandwidth	BW	1	Hz

the lower bound of which is the noise floor (in a 1 Hz bandwidth) and the upper bound of which is the value that produces distortion terms with output power equal to the noise floor [9], [11]. For sub-octave applications, the third order intermodulation distortion is of primary concern, while for broadband RF photonic links, both second-order and third-order harmonic distortions also should be taken into account [11].

Analytically, the third order intermodulation (IM3) SFDR can be expressed as [12], [13]:

$$SFDR_{IM3} = \frac{2}{3}(IP3_o - \text{noisefloor} - 10 \cdot \log_{10} \text{BW}) \quad (1)$$

Where $IP3_o$ indicates the output third-order interception point, which is an imaginary point where the fundamental and third order intermodulation response curves intersect [13]. The *noise floor* in the equation indicates the power level of the output noise in 1-Hz bandwidth. The equation for SHD SFDR and THD SFDR are similar except that the $IP3_o$ is replaced by the intercept point between the fundamental and SHD responses, and between the fundamental and THD responses, respectively. The coefficient outside of parenthesis is also different; it is 1/2 for the second order distortions (SHD) and 2/3 for the third order

(THD, IM3) distortions because of the different slopes of the distortion responses. From (1) it is clear that SFDR is determined by two factors: interception point $IP3_o$ which is decided by system linearity and noise floor (comprising RIN noise, shot noise, thermal noise and optical amplifiers added noise).

C. SFDR Dependence on Link Dispersion and Loss

Transmission media imperfections, such as loss, chromatic dispersion and nonlinearities, degrade the SFDR of an analog optical link in different ways [12]–[15]. While dispersion and loss can notably increase when changing the structure parameters, as shown in Fig. 2, the optical nonlinearities of the HCG-HW are maintained at a fairly low value (nonlinear coefficient $<10^{-7}$ W^{-1} km^{-1}) over a wide range of structure parameters [7], and therefore they hardly affect the analog signals.

The output power of a quadrature-biased (on positive slope), zero-chirp MZM fed by a CW laser is related to the applied RF signal V_{RF} (t) by a nonlinear relationship [16]:

$$P_{\mathrm{mod}}(t) \propto \left(1+\cos\left(\frac{\pi V_{\mathrm{RF}}(t)}{V_\pi}+\frac{3\pi}{2}\right)\right) = 1+\sin\left(\frac{\pi V_{\mathrm{RF}}(t)}{V_\pi}\right) \quad (2)$$

Thus, even in the absence of dispersion, the retrieved RF signal, being proportional to the photodetector output current/voltage, and therefore to $P_{\mathrm{mod}}(t)$, is already afflicted by distortions. Due to the odd symmetry of the sine function, SHD is minimized but THD is maximized.

The introduction of dispersion seriously aggravates the situation, particularly for signals with high modulation frequencies [15]. To explain, we first note that the sine function in (2) transforms every RF tone to multiple sidebands around the optical carrier, while the square-law photodetector retrieves the RF tones as a sum of beating terms, originating from pairs of optical sidebands, having the same frequency spacing. This summation critically depends on the relative phases of the various contributions, which are directly affected by dispersion. Thus, distortion terms that were missing from $P_{\mathrm{mod}}(t)$ are no longer zero. Similarly, originally weak terms may grow in magnitude.

Fig. 4 shows that dispersion induces a periodic change in the intensity of the fundamental RF carrier and distortion terms (including IM3, SHD and THD) with a modulation frequency of approximately 40 GHz ($f_1 = 40$ GHz, $f_2 = 41$ GHz). The period of each curve is determined by its frequency. Since the frequency of IM3 $(2f_1 - f_2)$ is very close to that of the RF carrier (f_1), they have similar periodicities. Therefore, the IM3 SFDR is relatively more tolerant to the variations in dispersion than SHD $(2f_1)$ and THD $(3f_1)$. The latter two are more sensitive to dispersion because they have double and triple frequency spacing, respectively. As expected, at the zero dispersion point, i.e., at the output of the modulator without transmission, SHD is minimized while THD is maximized. Therefore, with the increase of dispersion in a range of less than a half period (in this case <100 ps/nm/km), SHD increases faster and THD decreases even faster, as can be seen in Fig. 4. The second order intermodulation distortions (IM2), including $f_1 + f_2$ term and $f_1 - f_2$ term, are also analyzed in Fig. 4. It can be seen that IM2

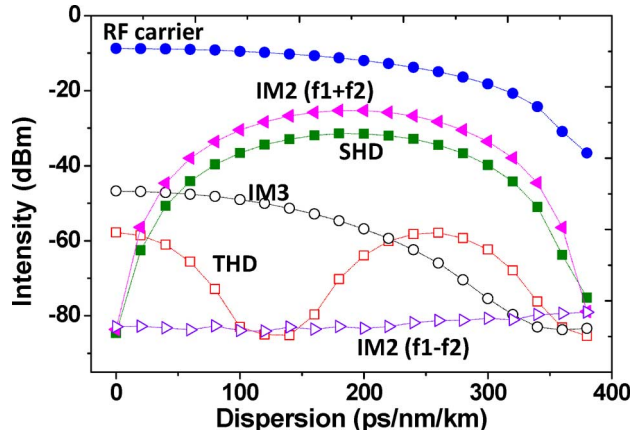

Fig. 4. Power of RF carrier and distortions as functions of dispersion. Modulation frequency: $f_1 = 40$ GHz, $f_2 = 41$ GHz. The propagation distance is 100 m.

$(f_1 + f_2)$ is a little stronger than the SHD, while they have a very similar dependence on the dispersion due to the fact that $f_1 + f_2 \approx 2f_1 \approx 2f_2$. The other one, IM2 $(f_1 - f_2)$, is much lower than other distortion terms during the analyzing range (i.e., dispersion is less than 400 ps/nm/km), and is therefore not considered in the later discussion.

The optical transmission loss may also induce notable reduction of the SFDR [9]. Equation (1) shows that the SFDR is determined by the $IP3_o$ and the power of noise. Provided that the nonlinearity of HCG-HW is negligibly low, $IP3_o$ is linearly related to the optical transmission loss, i.e., every 1 dB of optical loss results in a 2 dB reduction on the output power of the electrical signal (including RF carrier and distortions) after optical/electrical conversion according to the square law detection. However, the consequent reduction of the noise floor might not be always linear, depending on the source of the noise that is dominant at the output. Generally, in an optical link without an optical amplifier, the noise sources include mainly RIN noise, thermal noise and shot noise. Their relationships to the optical power incident to the photodetector (P_{opt}) are as follows [12]:

$$P_{\mathrm{RIN}} \sim P_{\mathrm{opt}}^2 \quad P_{\mathrm{Shot}} \sim P_{\mathrm{opt}} \quad P_{\mathrm{Thermal}} \sim T \quad (3)$$

where T indicates the temperature. From the equations above it can be seen that every 1 dB of optical loss causes 2 dB and 1 dB reductions on the power of RIN noise and shot noise (dark current is low enough and not considered here), respectively, and has no effect on the thermal noise since it is only related to the temperature T [11]. Different reductions in the power of output signal and noise floor will finally result in changes in SFDR. Fig. 5 shows the dependence of the second order and the third order SFDR on optical transmission loss. For an optical link with the parameters listed in Table I, a loss of 0–10 dB has almost no effect on the SFDRs because the system is dominated by RIN noise. Shot noise becomes the dominant noise when the loss is in the range of 10–20 dB. In this case, 1-dB loss might cause reductions in second-order SFDR and third-order SFDR of 0.5 and 0.67 dB, respectively. For a loss of more than 20 dB,

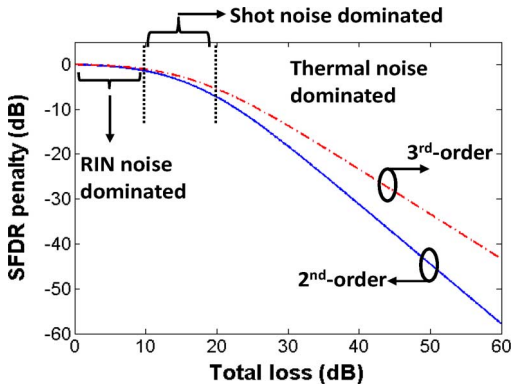

Fig. 5. SFDR reduction as a function of link loss. The 3rd-order includes IM3 SFDR and THD SFDR. The 2nd-order indicates the SHD SFDR.

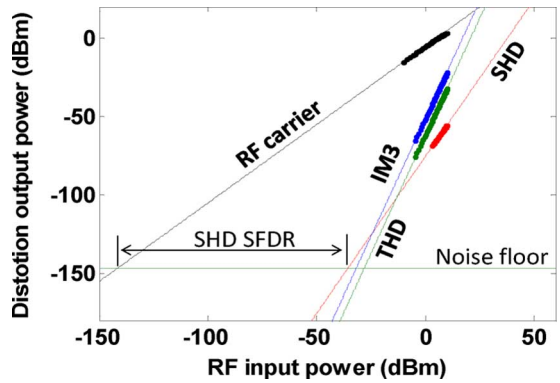

Fig. 6. Power of RF carrier and distortions as functions of RF input power. According to the definition, SFDRs can be obtained by measuring the interval between two intersections, as shown in the figure. The link using 100 m HCG-HW with optimized parameters can achieve a SHD SFDR of 105.7 dB· $Hz^{1/2}$, THD SFDR of 113.3 dB · $Hz^{2/3}$ and an IM3 SFDR of 109.9 dB · $Hz^{2/3}$ at 40 GHz.

thermal noise is most significant, and the reduction in the SFDRs caused by the optical loss should be doubled compared to the case in which shot noise is dominant.

Since the nonlinearity of HCG-HW is negligibly low [4], the dispersion and optical losses are the main contributors to changes in the SFDR of the link.

IV. Results and Discussions

A. SFDR and Bandwidth

Using the model described above, we first investigate the performance of a HCG-HW with optimized structure parameters, which are: core size 15 μm, air gap 430 nm, grating thickness 340 nm and period of 750 nm. Fig. 6 shows the intensity of RF carrier and distortions (IM3 and SHD) as functions of RF input power. SFDRs can be obtained by measuring intercepting points of the noise floor and each distortions terms, as shown in Fig. 6. Operating at 1550 nm, the IM3 and SHD SFDRs in a 100 m HCG-HW link are 109.9 dB ·$Hz^{2/3}$ and 105.7 dB ·$Hz^{1/2}$, respectively, at a modulation frequency of 40 GHz. The modulation frequency of around 40 GHz is used because the HCG-HW is relatively linear and we cannot see any notable distortions from the spectrum of the output analog signal with a lower frequency. The THD SFDR, which is also shown in this figure, is calculated as 113.3 dB · $Hz^{2/3}$. It is noted that the achieved IM3 SFDR of the analog link using HCG-HW is as high as that of a back-to-back analog link using a MZM [9], which shows the great linearity of the HCG-HW.

Broadening the operational RF bandwidth of an analog link is of great importance. Fig. 7 depicts the SFDRs as functions of the modulation rate, i.e., the frequency of the driving analog signal. When we change the modulation rate from 1 GHz to 80 GHz, IM3 SFDR remains almost constant at 109.9 dB · $Hz^{2/3}$, while SHD SFDR decreases as the modulation frequency increases, but, as shown in Fig. 7, it is still greater than 90 dB · $Hz^{1/2}$ at 80 GHz. THD SFDR is also quite independent of the modulation frequency, except for a small increase at the end, as shown in Fig. 7. As we know that dispersion induced phase shift (delay) is proportional to the signal bandwidth, therefore, increasing the modulation frequency in an analog link strengthens the effects of chromatic dispersion. As indicated in Section III

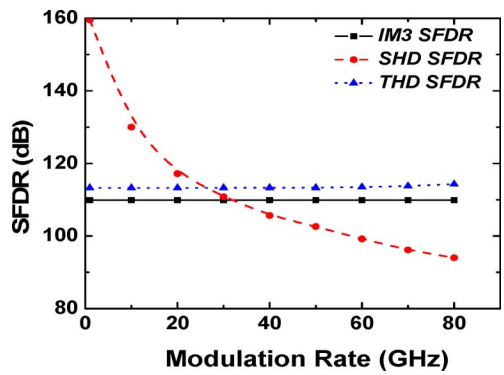

Fig. 7. SFDRs as function of modulation frequency. IM3 SFDR and THD SFDR have little change when the modulation rate is increased. However, SHD SFDR decreases significantly due to the chromatic dispersion of the HCG-HW.

concerning the dependence of SFDR on the dispersion (Fig. 3), IM3 and THD SFDRs are more tolerant to dispersion than SHD SDFR. At the zero point of the modulation rate, the SHD SFDR drops rapidly with modulation frequency. THD SFDR has a little improvement since the IM3 distortion is partly canceled due to the dispersion. These results also indicate that HCG-HW is promising for both sub-octave and broadband on-chip analog applications.

Optical bandwidth is also worthy of consideration for many applications, such as wavelength division-multiplexing (WDM). The SFDR dependence on operating wavelength is shown in Fig. 8. It can be seen that both THD and IM3 SFDR achieve the largest value at 1550 nm, where the waveguide has the minimum loss. However, the maximum value of SHD SFDR occurs at 1525 nm, which is the zero dispersion wavelength (ZDW) of HCG-HW. This again can be explained by the fact that SHD is dramatically affected by dispersion and waveguide dispersion changes with the wavelength. All three SFDRs decrease rapidly when the wavelength is out of C band because the waveguide loss becomes larger, as indicated in Fig. 8. However, an optical bandwidth of $\sim$50 nm with an all SFDRs greater than 85 (dB · $Hz^{1/2}$ for SHD and dB · $Hz^{2/3}$ for IM3 and THD) is still achieved.

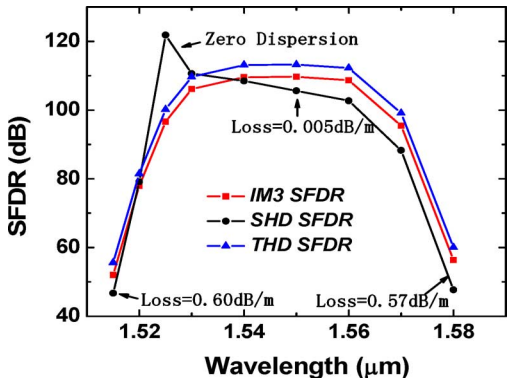

Fig. 8. SFDRs as functions of wavelength. HCG-HW shows an optical bandwidth of 50 nm with IM3 SFDR >100 dB $\cdot$ Hz $^{2/3}$ and SHD SFDR >85 dB $\cdot$ Hz$^{1/2}$.

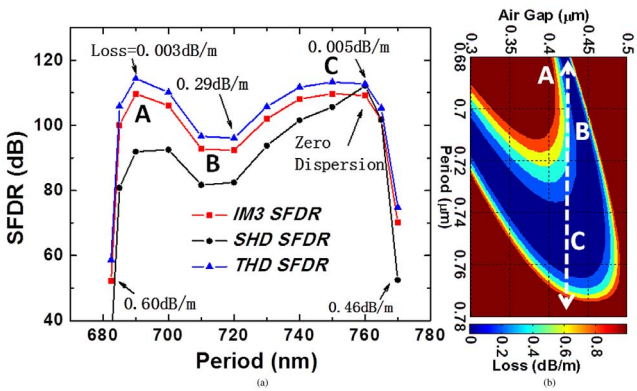

Fig. 9. (a) SFDRs as functions of grating period. (b) Calculated propagating loss as a function of grating period and air gap. The dotted arrow indicates the trace of changing period while keep the air gap at 470 nm. Two peaks of SFDR occur at period of around 690 nm and 750 nm, which correspond to two low-loss areas.

B. Grating Parameter Dependence

The results in Section A show that an optimally designed HCG-HW can potentially provide a good transmission medium for analog signals. However, from the waveguide structure shown in Fig. 1 we can see that there are different parameters that are highly related to the waveguide design, and it would be of great importance to investigate the dependence of the quality of the transmitted analog signal on each structure parameter. First, we calculate SFDR by varying a single grating parameter (grating period or air gap) each time, as shown in Fig. 9 and Fig. 10.

SFDRs as functions of grating period are shown in Fig. 9(a). The propagation loss of HCG-HW as a function of period and air gap is also depicted in Fig. 9(b) to help explain the curves. The dotted line in Fig. 9(b) is the trace of varying grating period while keeping the air gap at 430 nm without changing. The maximum value of IM3 SFDR and THD SFDR are achieved at grating period of $\sim$690 nm, where the waveguide has minimum loss. Note that there are two peaks (Point A and point C in Fig. 9(a)) at grating period of around 690 nm and 750 nm for all SFDR curves, corresponding to two low-loss areas (Point A and point C in Fig. 9(b)) respectively in the loss contour map on the right, with a dip in the middle (Point B). The effect of

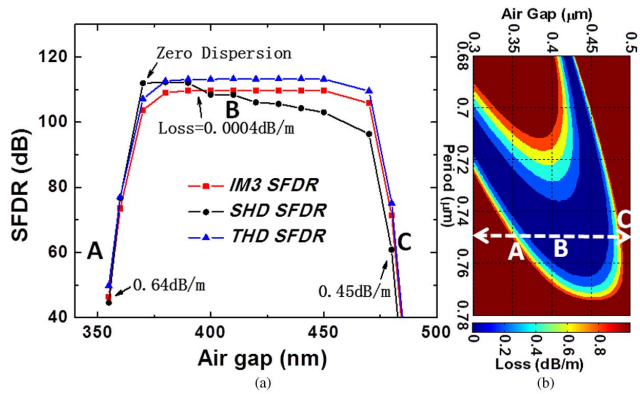

Fig. 10. (a) SFDR as function of grating air gap. (b) Calculated propagating loss as a function of grating period and air gap. The dotted arrow indicates the trace of changing air gap while keep the period at 750 nm. IM3 and THD SFDR are almost flat within the low loss region between 370 nm to 470 nm of air gap. SHD SFDR drops $\sim$10 dB with air gap due to the dispersion.

waveguide dispersion can be found from the SHD SFDR curve more obviously than the other two. Basically the WG dispersion increases as the period increases, thus the SHD SFDR peak at 690 nm is lower than that at 750 nm. The largest value of SHD SFDR is achieved at the grating period of $\sim$758 nm, where the waveguide has zero dispersion. At the grating period of beyond point A and point C, all SFDRs drop very rapidly due to the increase of waveguide loss, as can be seen from Fig. 9(b).

Fig. 10(a) shows SFDRs as functions of grating air gap. IM3 SFDR and THD SFDR are almost flat and kept at the maximum value of 109.9 dB $\cdot$ Hz $^{2/3}$ within the range of between 370 nm and 470 nm, while SHD SFDR has a $\sim$10 dB drop with the increase of grating air gap due to its sensitivity on dispersion. Similarly, point A, B and C in Fig. 10(a) are corresponding to point A, B and C in the loss contour map, as shown in Fig. 10(b). The dotted line indicates the trace of changing air gap while keeping the period at 750 nm. Again, the rapid increase of waveguide loss beyond the air gap range of between 370 nm and 470 nm results in sharp declines of all three SFDRs, as shown in Fig. 10(a).

C. Fabrication Tolerance & Comparison With Silicon WGs

For a waveguide with submicron gratings, the accuracy of fabrication is an important factor that should be taken into account. In the last section we discuss the waveguide performance variations caused by changing a single structure parameter. In a more realistic case, all three grating parameters (air gap, period and thickness) might change simultaneously and affect waveguide performances significantly. In order to characterize the fabrication tolerance of HCG-HW, we generate a "parameter cube" with Period, Thickness and Air gap as its three axes of the coordinate, as shown in Fig. 11. The center of the cube is considered as the operating point with optimized parameters, i.e., air gap (a_g) of 430 nm, grating thickness (t_g) of 340 nm and period (Λ) of 750 nm. Each of these three parameters might have a variation of $+/-10$ nm or $+/-20$ nm, thus there are eight combinations of three parameters, which can be indicated by eight vertices, respectively, among which the worst one (with the smallest SFDR) could be considered as the lower bound of all points inside the cube. This is reasonable, because within the

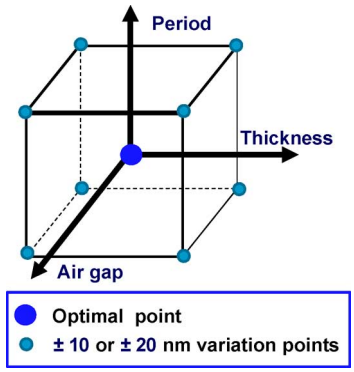

Fig. 11. Parameter cube of the HCG-HW. The optimal point indicates the HCG-HW with the optimized parameters, i.e., core size (D) of 15 μm, air gap (a_g) of 430 nm, grating thickness (t_g) of 340 nm and period (Λ) of 750 nm.

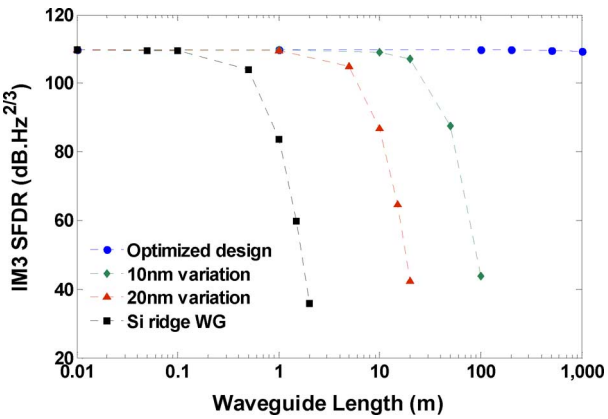

Fig. 12. IM3 SFDR as a function of propagating length in an HCG-HW.

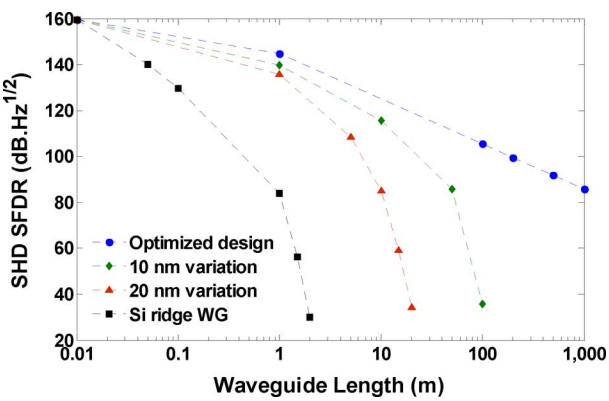

Fig. 13. SHD SFDR as a function of propagating length in an HCG-HW.

10 nm and 20 nm range, the loss, dispersion and nonlinear of HCG-HW change monotonously. Then we calculate the SFDR as a function of the length of the waveguide in the cases of optimized point, ± 10 nm variation and ± 20 nm variation, as shown in Fig. 11, which can give us a comprehensive picture of the performance of HCG-HW in terms of fabrication tolerance.

Figs. 12 and 13 show IM3 SFDR and SHD SFDR as a function of propagation distance, respectively. The results indicate that an HCG-HW with the optimal design performs fairly well. However, the waveguide performance can be affected significantly by the parameter changes. With a fabrication variation of ± 10 nm, the propagation distance is limited to ~ 28 m to achieve an IM3 SFDR of >100 dB $\cdot$ Hz$^{2/3}$. The distance is further decreased to ~ 6 m when there is a ± 20 nm variation on the waveguide parameters. Similar trends can be observed in Fig. 13. To maintain a SHD SFDR of >100 dB $\cdot$ Hz$^{1/2}$, the propagation length is limited to ~ 22 m and ~ 6.5 m, with a parameter variation of ± 10 nm and ± 20 nm, respectively.

Focusing on the analog signaling performance, we make a simple comparison between a HCG-HW and low-loss silicon ridge waveguides [17], [18], as shown in Figs. 12 and 13. The SFDRs of a low-loss silicon ridge waveguide as functions of transmission distance are calculated. It seems that even with a ± 20 nm variation in all three grating parameters, HCG-HWs still perform better than silicon-ridge waveguides.

V. Conclusion

In this paper, we investigate the performance of an HCG-HW for the transmission of analog signals. The simulation results indicate that an HCG-HW with optimized parameters has a RF bandwidth of up to 80 GHz and a operating wavelength range of >50 nm, with an IM3 SFDR of greater than 100 dB $\cdot$ Hz$^{2/3}$. Analysis also implies that HCG-HW performance is dependent on the waveguide structure parameters. To maintain a IM3 SFDR of >100 dB $\cdot$ Hz $^{2/3}$, the analog signal propagation distance is limited to ~ 6 m due to a ± 20 nm variation on all three parameters.

Acknowledgment

This work is sponsored by the Defense Advanced Research Projects Agency (DARPA) Integrated Photonic Delay (iPhoD) program (under contract number HR0011-09-C-0124).

References

[1] C. H. Cox, III, *Analog Optical Links: Theory and Practice*. : Cambridge University Press, 2004, pp. 201–205.
[2] W. S. C. Chang, *RF Photonic Technology in Optical Fiber Links*. : Cambridge University Press, 2002, pp. 25–32.
[3] P. Roberts, "Ultimate low loss of hollow-core photonic crystal fibers," *Optics Express*, vol. 13, no. 1, pp. 236–244, Jan. 2005.
[4] Y. Zhou, V. Karagodsky, B. Pesala, F. G. Sedgwick, and C. J. Chang-Hasnain, "A novel ultra-low loss hollow-core waveguide using subwavelength high-contrast gratings," *Optics Express*, vol. 17, no. 3, pp. 1508–1517, 2009.
[5] V. Karagodsky, F. G. Sedgwick, and C. J. Chang-Hasnain, "Theoretical analysis of subwavelength high contrast grating reflectors," *Optics Express*, vol. 18, no. 16, pp. 16973–16988, 2010.
[6] Y. Yue, L. Zhang, J. Wang, Y. Xiao-Li, B. Shamee, V. Karagodsky, F. G. Sedgwick, W. Hofmann, R. G. Beausoleil, C. J. Chang-Hasnain, and A. E. Willner, "A 'linear' high-contrast gratings hollow-core waveguide and its system level performance," presented at the The Optical Fiber Commun. Conf. (OFC), San Diego, CA, 2010, presented at, paper OTuI5.
[7] Y. Yue, L. Zhang, F. G. Sedgwick, B. Shamee, W. Yang, J. Ferrara, C. Chase, R. G. Beausoleil, C. J. Chang-Hasnain, and A. E. Willner, "Chromatic dispersion variation and its effect on high-speed data signals due to structural parameter changes in a high-contrast-grating waveguide," presented at the The IEEE Photonics Society Annual Meeting, Denver, CO, 2010, presented at, paper ThB2.
[8] H. Huang, Y. Yue, L. Zhang, X. Wang, C. Chase, D. Parekh, F. Sedgwick, M. Tur, M. C. Wu, C. J. Chang-Hasnain, and A. Willner, "Analog signal performance of a hollow-core-waveguide using high-contrast-gratings," presented at the The Optical Fiber Commun. Conf. (OFC), Los Angeles, CA, 2011, presented at, paper OThA3.

[9] W. B. Bridges and J. H. Schaffner, "Distortion in linearized electrooptic modulators," *IEEE Transations on Microwave Theory and Techniques*, vol. 43, no. 9, pp. 2184–2197, Sept. 1995.
[10] B. Pesala, V. Karagodsky, and C. Chang-Hasnain, "Ultra-compact low loss photonic components using high-contrast gratings," presented at the ICOP 2009-International Conference on Optics and Photonics CSIO, Chandigarh, India, 2009, presented.
[11] C. H. Cox, III, E. I. Ackerman, G. E. Betts, and J. L. Prince, "Limits on the performance of RF-over-fiber links and their impact on device design," *IEEE Transactions on Microwave Theory and Techniques*, vol. 54, no. 2, pp. 906–920, Feb. 2006.
[12] G. Katz, S. Arnon, P. Goldgeier, Y. Hauptman, and N. Atias, "Cellular over optical wireless networks," *IEE Proceedings—Optoelectronics*, vol. 153, no. 4, pp. 195–198, Aug. 2006.
[13] J. A. MacDonald, M. V. Kubak, and A. Katz, "Wideband dynamic range improvement of microwave photonic links," presented at the IEEE Conference, Avionics Fiber-Optics and Photonics, Minneapolis, MN, Sept. 20–22, 2005, presented, paper ThB3, pp. 67–68.
[14] G. J. Meslener, "Chromatic dispersion induced distortion of modulated monochromatic light employing direct detection," *IEEE Journal of Quantum Electronics*, vol. 20, no. 10, pp. 1208–1216, Oct. 1984.
[15] C. S. Oh and W. Gu, "Fiber induced distortions in a subcarrier multiplexed lightwave system," *IEEE Journal on Selected Areas in Communications*, vol. 8, no. 7, pp. 1296–1303, Sept. 1990.
[16] G. K. Gopalakrishnan, W. K. Burns, and C. H. Bulmer, "Microwave-optical mixing in LiNbO3 modulators," *IEEE Transactions on Microwave Theory and Techniques*, vol. 41, no. 12, pp. 2383–2391, Dec. 1993.
[17] R. Pafchek, R. Tummidi, J. Li, M. A. Webster, E. Chen, and T. L. Koch, "Low-loss silicon-on-insulator shallow-ridge TE and TM waveguides formed using thermal oxidation," *Applied Optics*, vol. 48, no. 5, pp. 958–963, 2009.
[18] M. A. Webster, R. M. Pafchek, G. Sukumaran, and T. L. Koch, "Low-loss quasi-planar ridge waveguides formed on thin silicon- on-insulator," *Applied Physics Letters*, vol. 87, no. 23, 2005.

Author biographies not included by author request due to space constraints.